

MICROSTRUCTURE-RELATED Pb^{2+} ADSORPTION CAPABILITY OF Ti-PILLARED MONTMORILLONITE IN AQUEOUS SOLUTION

JINGYI LIU¹, RUI CHEN¹, YURU LI¹, JIAJIA CHEN¹, LIHUI CHEN¹, JING GAO^{1,2}, AND GUOHUA LI^{1,2,*}

¹ School of Chemical Engineering, Zhejiang University of Technology, Hangzhou 310032, P.R. China

² State Key Breeding Base of Green Chemistry Synthesis Technology, Hangzhou 310032, P.R. China

Abstract—The elimination of Pb^{2+} and recovery of lead metal during the treatment of industrial sewage is an important research topic. Montmorillonite (Mnt) is a promising material in this regard. The purpose of the present study was to improve the Pb^{2+} adsorption ability of Na-containing Mnt (Na-Mnt) by pillaring titania (anatase) into its interlayer spaces using a sol-gel method. The samples were characterized by X-ray diffraction (XRD), scanning electron microscopy (SEM), and transmission electron microscopy (TEM). The ratio of Ti to Mnt affected the crystal phase of titania-pillared Na-Mnt (Ti-Mnt), and changed the interlayer spacing of the (001) plane of Ti-Mnt and the growth of anatase. The Pb^{2+} -adsorption capabilities of Ti-Mnt were tested using an aqueous solution of lead nitrate as a wastewater model. The Ti-Mnt prepared adsorbed >99.99% of the Pb^{2+} ; leached and activated Ti-Mnt adsorbed >95.7% of the Pb^{2+} , indicating that Ti-Mnt could be recycled effectively. Furthermore, the Pb^{2+} -adsorption capability of Ti-Mnt was related to the interlayer spacing of Mnt, the distribution of anatase particles pillared in Mnt, and the specific surface area, especially with respect to the relationship between the anatase particles and the interlayer spacing of the (001) plane.

Key Words—Adsorptive Capability, Anatase, Montmorillonite, Microstructure, Pillar, Relativity.

INTRODUCTION

Pb^{2+} in industrial wastewater is very harmful to human health and plant growth; the removal of Pb^{2+} and the recovery of lead metal from industrial wastewater is a major challenge in protecting the environment. In the treatment of industrial wastewater, direct adsorption of Pb^{2+} is viewed as the simplest and most economical approach. Activated carbon is used widely as an adsorbent to this end. The cost of the activated carbon, compared to natural adsorbents, limits its utilization, however; natural adsorbents such as montmorillonite (Mnt) are promising alternative candidates for adsorption of Pb^{2+} . Mnt is an important natural silicate mineral with a lamellar structure but its small particle size and variable interlayer spacing lead to low porosity. By placing pillars of metal oxides in the interlaminar spaces of Mnt (known as ‘pillaring’), the interlayer spacing can be homogenized and stabilized, the particle size enlarged, and the porosity increased. Numerous efforts have been made to expand the interlayer spacing of the (001) plane of Mnt to increase its specific surface area and to improve its adsorption capability for potential applications (Fetter *et al.*, 1997; Korosi *et al.*, 2004; Yaron-Marcovich *et al.*, 2005; Hur *et al.*, 2006; Miao *et al.*, 2006; Tabet *et al.*, 2006; Zhou, 2011; Zhou and Keeling, 2013; Zhou *et al.*, 2016).

Recently, titania has been pillared into the interlayers of Mnt to form a Ti-Mnt nanocomposite (Chen *et al.*, 2013; Tahir *et al.*, 2013; Djellabi *et al.*, 2014; Zhang *et al.*, 2014; Tahir *et al.*, 2015; Barama *et al.*, 2017; Mulewa *et al.*, 2017). These composites have been studied extensively to achieve better photocatalytic activity. Ti-Mnt also exhibits excellent stability (Mulewa *et al.*, 2017), reusability (Djellabi *et al.*, 2014; Zhang *et al.*, 2014), and adsorption capability (Djellabi *et al.*, 2014). As a result, Ti-Mnt is viewed as a low-cost alternative adsorbent for wastewater treatment. The application of Ti-Mnt in the treatment of Pb^{2+} -containing wastewater has rarely been investigated, however (Liang, 2013; Irannajad *et al.*, 2017).

During the present study, the relationship between the microstructure of Ti-Mnt and its Pb^{2+} adsorption capability in aqueous solution were investigated. The Pb^{2+} adsorption capability of Mnt was improved by Ti-pillaring. This improvement is related to the enlargement of the interlayer spacing, the loose layer structure of the (001) plane, well dispersed anatase particles, and sufficient active sites for adsorption which are provided by both the Mnt layer and anatase particles. Ti-Mnt with adsorbed Pb^{2+} could also be recycled easily using a nitric acid solution to leach out Pb^{2+} .

EXPERIMENTAL

Chemicals

Butyl titanate (CP) was purchased from Aladdin (Tianjin, China). Sodium-containing montmorillonite (Na-Mnt) was purchased from Sand Technology Co. Ltd. (Anji, Zhejiang, China). Nitric acid (analytical

* E-mail address of corresponding author:

nanozjut@zjut.edu.cn

DOI: 10.1346/CCMN.2018.064112

grade, AR) and absolute ethyl alcohol (AR) were purchased from Aladdin (Tianjin, China). All chemicals were used without further purification.

Sample preparation

The Ti-Mnt nanocomposite was prepared in two steps: (1) preparation of pillaring solution; and (2) pillaring the Na-Mnt with the solution. The pillaring solution was prepared as follows: first, 100 mL of butyl titanate was added dropwise to 100 mL of absolute ethyl alcohol under stirring at 0°C to obtain solution A. This solution was stirred at room temperature for 30 min. Next, 40 mL of HNO₃ (1.0 mol/L) was added dropwise to 25 mL of absolute ethyl alcohol under stirring at 0°C to prepare an acidic solution (S_A). Then, 40 mL of NaOH (1.0 mol/L) was added dropwise to 25 mL of absolute ethyl alcohol under stirring at 0°C to prepare an alkaline solution (S_B). Finally, solution A was added dropwise to S_A and S_B under stirring at 0°C. The acidic and alkaline pillaring solutions were named P_A and P_B, respectively.

The samples were prepared as follows: first, 10 g of Na-Mnt was dispersed in 1000 mL of deionized water under stirring at room temperature to obtain a suspension liquid. Secondly, pillaring solution P_A or P_B was added dropwise to the suspension at various temperatures (0–20°C) and stirred for 3 h, followed by aging for 24 h. A certain amount of pillaring solution P_A or P_B was added to adjust the ratio of Ti:Mnt to between 0.3 and 2.0 (mmol/g). The mixed liquid was filtered to obtain a filtered cake. The cake was rinsed six times with deionized water and once with absolute ethyl alcohol, dried at 80°C overnight, and calcined at 500°C for 4 h to obtain pillared Mnt powder.

Measurement of properties

A solution with a Pb²⁺ concentration of 1000.0 mg/L was obtained by adding 1.60 g of Pb(NO₃)₂ to a 100 mL volumetric flask and dissolving it with deionized water to the mark of the flask. Similarly, 1.60 g of Pb(NO₃)₂ was added to a 1000 mL volumetric flask and dissolved by deionized water to the mark of the flask to obtain another solution with a Pb²⁺ concentration of 100.0 mg/L. Adsorption tests were carried out according to the following steps. The Pb²⁺ solutions prepared were used as models of wastewater. 0.2 g of Ti-Mnt was added to 100 mL of the Pb²⁺ solutions (1000.0 and 100.0 mg/L) and stirred for 30 min to form two suspension liquids. The Ti-Mnt sat in the two liquids at room temperature for 2 h, and then the liquids were centrifuged at 5600 × g. Finally, the concentrations of the remaining Pb²⁺ in the liquids were measured by flame atomic absorption spectroscopy (FLAAS). The Pb²⁺ adsorption efficiency of the Ti-Mnt was calculated according to the following equation:

$$\text{Adsorption capability (\%)} = (C_0 - C_1)/C_0 \times 100\% \quad (1)$$

where C_0 and C_1 are the initial and equilibrium concentrations of Pb²⁺ in the aqueous solution, respectively. For the control experiment, 0.2 g of Na-Mnt and 0.2 g of anatase nanoparticles prepared by a sol-gel method were subjected to the same procedure.

To investigate the recyclability of the sample, a leaching experiment was carried out using nitric acid solution as a leaching agent. Firstly, 10 mL of nitric acid solution with a concentration of 1.0 mol/L was prepared. Secondly, Ti-Mnt was centrifuged after an adsorption experiment and then added to the nitric acid solution under stirring. After 15 min, a suspension liquid formed. The suspension liquid was kept for 2 h and then centrifuged at 5600 × g. Finally, the Pb²⁺ concentrations in the nitric acid solution were measured by FLAAS. The Pb²⁺-leaching ratio from the Ti-Mnt was calculated as follows:

$$\text{Leaching ratio (\%)} = C_2/(C_0 - C_1) \times 100\% \quad (2)$$

where C_2 is the Pb²⁺ concentration in the nitric acid solution after the leaching experiment.

The centrifuged Ti-Mnt after the leaching experiment was rinsed with deionized water six times and with absolute ethanol once and then dried at 80°C overnight to obtain sample 1. This sample was then activated at 100°C for 1 h to obtain sample 2. Next, 0.2 g of sample 1 and sample 2 were added to 100 mL of aqueous Pb²⁺ solution (1000.0 mg/L). A liquid suspension formed after stirring at room temperature for 2 h. The suspension was centrifuged at 5600 × g. The remaining Pb²⁺ concentrations in the liquids were measured by FLAAS. The adsorption efficiency of the leached and activated Ti-Mnt was calculated according to equation 1.

RESULTS AND DISCUSSION

XRD

Acid or alkaline pillaring solution was added to the Na-Mnt suspension with a Ti:Mnt ratio of 1.0 (mmol/g) (Figure 1) at 5°C; then the anatase was pillared successfully into Na-Mnt, consistent with a previous report by Tahir and Amin (2013). The diffraction peaks of anatase in the Ti-Mnt pillared in alkaline solution were not as obvious as expected, however, possibly because that part of the titania pillared into the Mnt was amorphous (Mogyorosi, *et al.*, 2003). Furthermore, the crystal planes of anatase in the Ti-Mnt pillared in alkaline solution are more complex than those pillared in acidic solution (Figure 1). Specifically, the diffraction peaks of the (101), (004), (200), (105), and (204) planes of anatase in the Ti-Mnt pillared in acidic solution are much clearer than those pillared in alkaline solution except for the (213) plane of anatase. This indicates that the crystallinity of the anatase pillared in acidic solution is greater than that pillared in alkaline solution. The results suggest that the development of the crystal planes of anatase pillared in acidic solution is different from that pillared in alkaline solution.

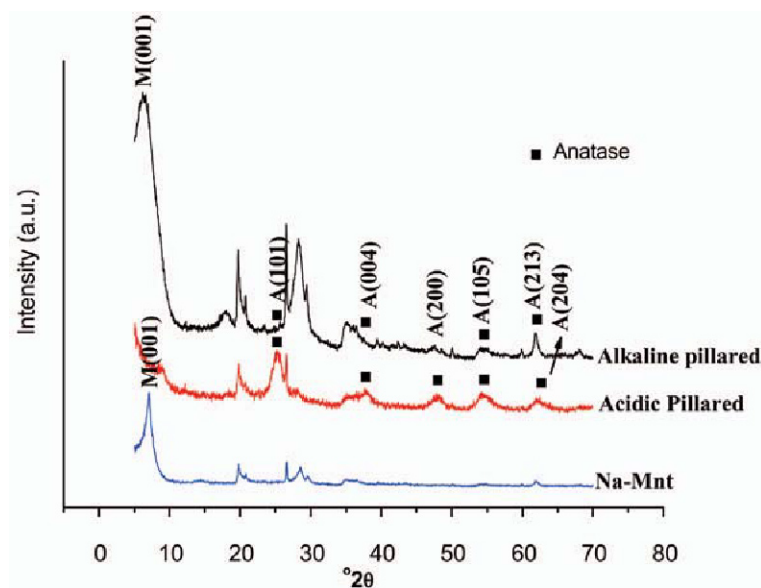


Figure 1. XRD patterns of Na-Mnt and Ti-Mnt prepared under acidic or alkaline conditions. M: Montmorillonite (Mnt); A: anatase; (001): crystal plane (001).

Compared to the diffraction peak of the (001) plane of Na-Mnt, the corresponding diffraction peak of Ti-Mnt pillared in alkaline solution shifted slightly to a lower angle (Figure 1). According to the Scherrer formula, the interlayer spaces of the (001) plane of Na-Mnt and Ti-Mnt pillared in alkaline solution were estimated to be 1.219 and 1.529 nm, respectively. These results are consistent with those reported by Ooka *et al.* (2003), indicating that anatase particles were located in the interlayer spaces of the Na-Mnt. This resulted in enlargement of the interlayer spacing of the (001)

plane of Ti-Mnt. Based on these results, the Ti-Mnt pillared in alkaline solution was selected to adsorb Pb^{2+} ions from wastewater.

To investigate the dependence of the pillaring temperature on the crystal phase of Ti-Mnt, the Ti-Mnt was pillared at 0, 5, 10, 15, and 20°C with a Ti:Mnt ratio of 1.0 (mmol/g) and then calcined at 500°C for 4 h. The Ti-Mnt pillared at various temperatures showed similar XRD patterns (Figure 2). This implies that the crystal phase was not affected by the pillaring temperature, which is consistent with previous reports (Chen *et al.*,

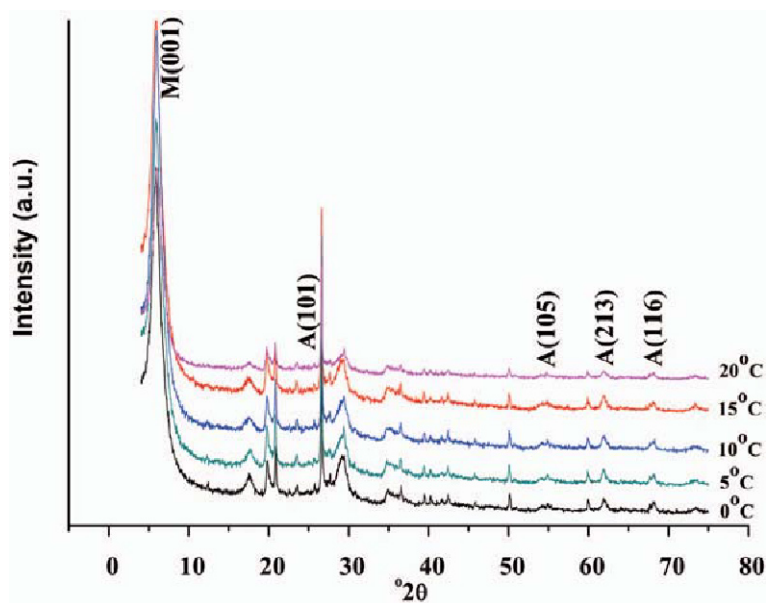


Figure 2. XRD patterns of Ti-Mnt pillared in alkaline solution at various temperatures.

2013; Sun *et al.*, 2015).

To study the dependence of the Ti:Mnt ratio on the crystal phase of Ti-Mnt, the Ti-Mnt was pillared with ratios of 0.3, 0.7, 1.0, 1.6, and 2.0 at 5°C and then calcined at 500°C for 4 h. The Ti-Mnt with various ratios exhibited similar diffraction peaks (Figure 3), implying that the crystal phase was not obviously affected by the ratio. According to the Scherrer formula, the interlayer spacing of the (001) plane of the Ti-Mnt with ratios of 0.3, 0.7, 1.0, 1.6, and 2.0 were estimated to be 1.288, 1.529, 1.307, 1.437, and 1.414 nm, respectively. These results show that the interlayer spacing of Ti-Mnt was not related linearly to the Ti:Mnt ratio, implying that the ratio is not the only factor in the interlayer spacing of the (001) plane during the pillaring process.

The order of diffraction intensity of the crystal planes of anatase is known to be: (101) > (200) > (004) = (105) = (211) (JCPDS#21-1272). When anatase was pillared into Ti-Mnt, however, the diffraction peaks of the (200) and (004) planes of anatase were not observed clearly, while distinct (213), (204), and (116) planes were obtained (Figures 1, 2, 3). These results indicate that the growth of anatase crystallite pillared into Ti-Mnt was transformed, which can be attributed to the pillaring of the crystallite in the interlayer space and the typical structure of the basal surface of Mnt (Underwood *et al.*, 2016).

SEM

A layered structure was observed clearly in the Na-Mnt and Ti-Mnt pillared at 5°C with various Ti:Mnt ratios calcined at 500°C for 4 h (Figure 4). The layer structure of Na-Mnt was tight (Figure 4a), and the layer surfaces were smooth and clean (Figure 4b). The layer structure of Ti-Mnt was loose, however, and some

irregular aggregates were observed on the layer surface (Figures 4c, d). These results confirm that the layer and surface structures of the Ti-Mnt had been altered. Furthermore, with the XRD patterns, the anatase particles were clearly pillared into the interlayer space of Mnt, leading to an enlargement of the layer distance of the (001) plane of Na-Mnt.

TEM

The TEM images of Na-Mnt and Ti-Mnt pillared at various ratios showed that the microstructures changed with the ratios (Figure 5). The layer structure of Na-Mnt was tight (Figure 5a), and no particles were observed on the layer surface (Figure 5a inset). This is consistent with the SEM results (Figure 4).

The layer structure of Ti-Mnt prepared at a ratio of 0.3 became loose (Figure 5b), and almost no particles were observed on the layer surface (Figure 5b inset). These observations are consistent with the XRD results, where no obvious diffraction peaks of anatase were detected. As the ratio of Ti to Mnt increased to 0.7, some particles were observed on the surface of the Ti-Mnt (Figure 5c).

Compared to Na-Mnt and Ti-Mnt pillared with a Ti:Mnt ratio of 0.3, the microstructures of Ti-Mnt pillared with ratios of >0.7 changed significantly (Figures 5c–f insets). When the Ti:Mnt ratio increased to 1.0, some particles assigned to anatase (according to the XRD results) were pillared into the interlayer spaces of Ti-Mnt (Figure 5d). When the Ti:Mnt ratio increased to 1.6, most of the anatase particles were pillared into the interlayer spaces of Ti-Mnt, while a small portion of the particles were found on the surface of the Ti-Mnt layer. The layers of Ti-Mnt were obviously pillared apart (Figure 5e), compared to the other ratios. When the

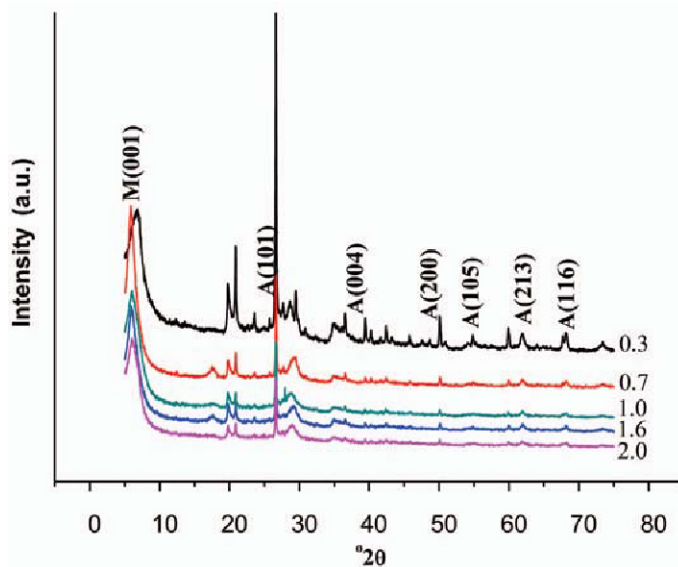


Figure 3. XRD patterns of Ti-Mnt pillared with various ratios of Ti to Mnt (mmol/g).

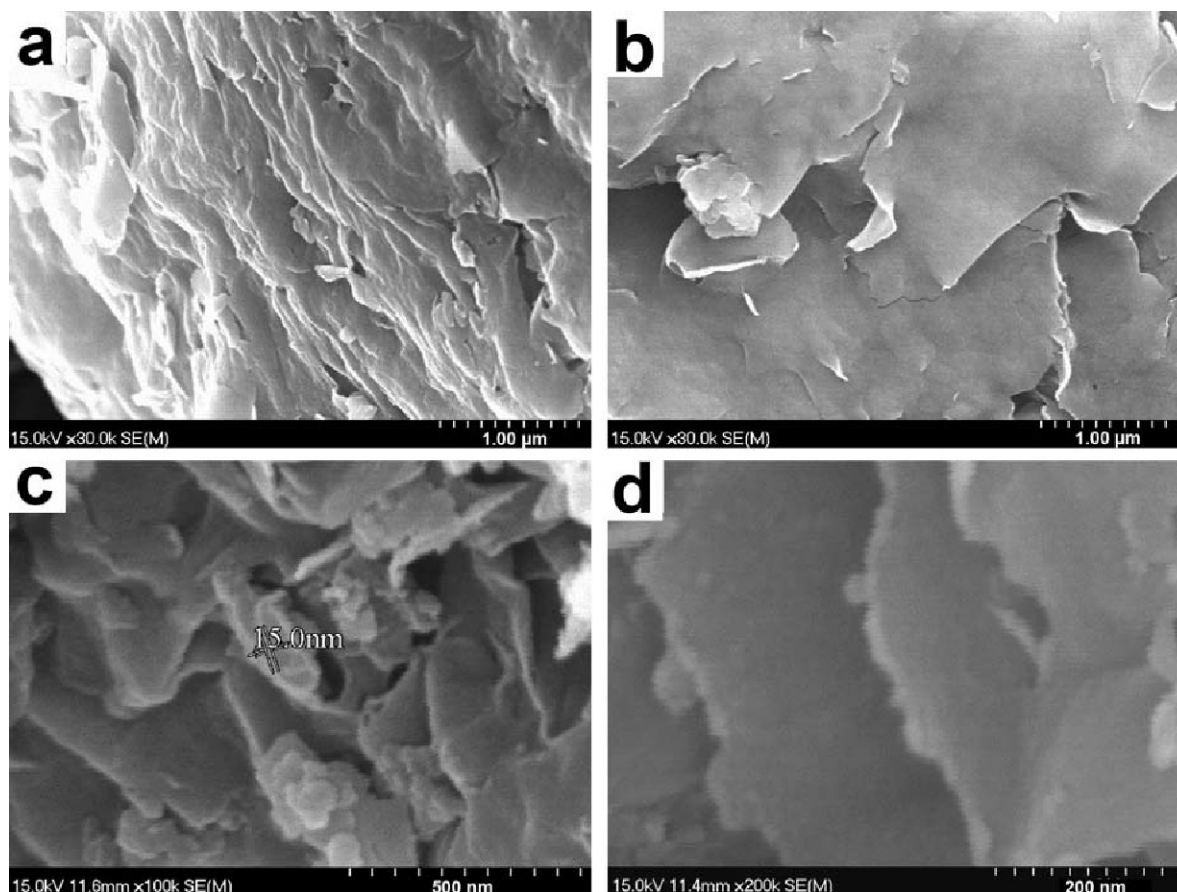


Figure 4. SEM images of Na-Mnt (a,b) and Ti-Mnt (c,d).

Ti:Mnt ratio increased to 2.0, anatase particles were pillared into the interlayer spaces and aggregated beyond the interlayer space (Figure 5f). The TEM results show that the distribution of anatase particles in Ti-Mnt is related to the Ti:Mnt ratio. Furthermore, the relationship between anatase particles and the interlayer space of Mnt can be adjusted by changing the ratio of Ti to Mnt.

Brunauer-Emmett-Teller (BET) results

Compared to Na-Mnt, the specific surface areas of Ti-Mnt with various Ti:Mnt ratios increased significantly (Table 1). When the ratio of Ti:Mnt was <2.0, the specific surface area of Ti-Mnt decreased with increasing interlayer distances. When the ratio of Ti:Mnt was 2.0, the specific surface area of Ti-Mnt was the greatest noted during the present experiments. The decrease in

surface area can be attributed to the separately pillared layers of Mnt (Figure 5e). The increase in surface area may result from anatase nanoparticles distributed beyond the Mnt at the Ti:Mnt ratio of 2.0 (Figure 5f).

Adsorption properties

The Pb^{2+} adsorption efficiency was >99.9% for Ti-Mnt and 88.6% for Na-Mnt (Table 2), indicating that the Pb^{2+} adsorption capability of Na-Mnt can be improved by titania pillaring. The adsorption efficiency of anatase nanoparticles prepared by the sol-gel method was only 2.3%, however. The improvement in the Pb^{2+} adsorption capability of Ti-Mnt can be attributed to the enlargement of the interlayer spacing of the (001) plane (Table 2).

The Pb^{2+} leaching ratio of Ti-Mnt containing absorbed Pb^{2+} was 84.8% (Table 3), indicating that the

Table 1. The surface area and interlayer distance of Ti-Mnt pillared with various Ti:Mnt ratios.

Ti:Mnt	Na-Mnt	0.7	1.0	1.6	2.0
Total surface area (m^2/g)	24.7	51.4	46.5	32.6	326.3
Basal spacing (001) (nm)	1.219	1.529	1.307	1.437	1.414

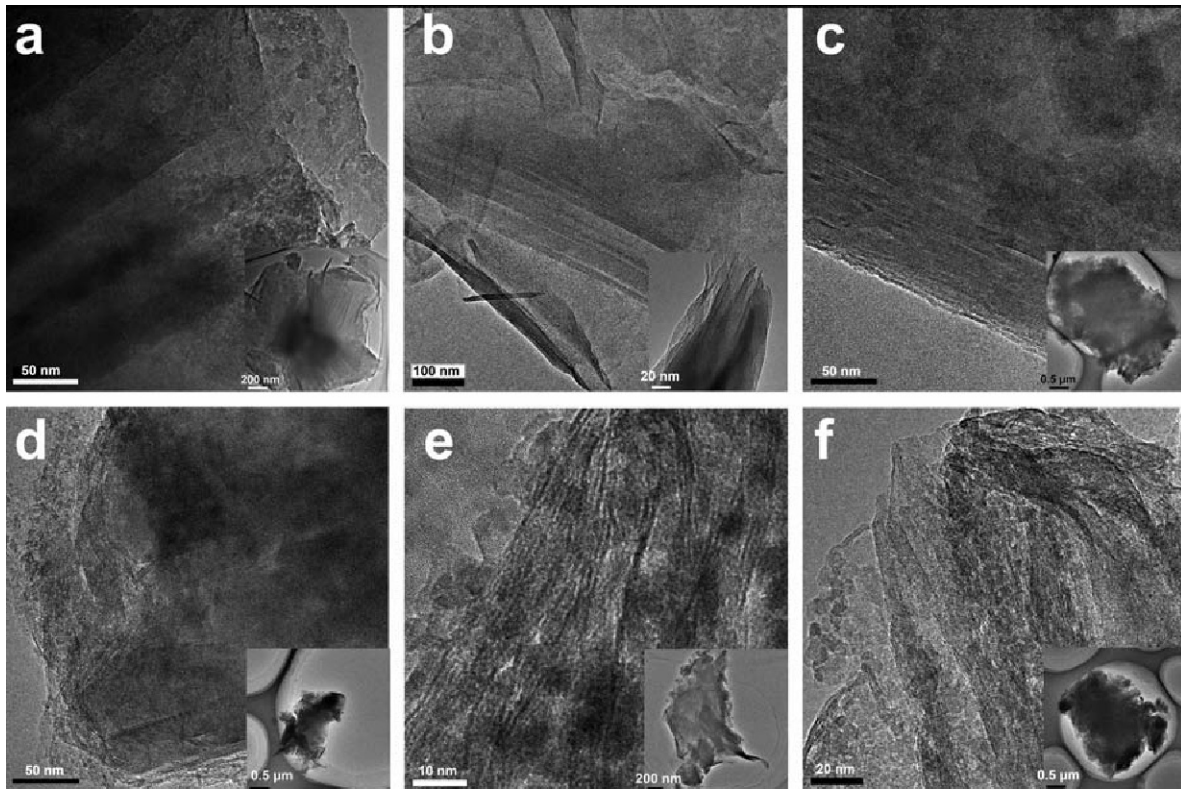


Figure 5. TEM images of Na-Mnt and Ti-Mnt (a) with various Ti:Mnt ratios: (b) 0.3, (c) 0.7, (d) 1.0, (e) 1.6, and (f) 2.0.

Pb²⁺ adsorbed can be leached efficiently by nitric acid solution. The Pb²⁺ adsorption efficiencies of Ti-Mnt, leached Ti-Mnt (sample 1), and activated Ti-Mnt (sample 2) were >99.9%, 95.7%, and 96.0%, respectively (Table 4). These results show that Ti-Mnt can be recycled easily *via* leaching of adsorbed Pb²⁺ by nitric

acid solution. This conclusion is consistent with previous results reported by Zhang *et al.* (2014) and Djellabi *et al.* (2014). Furthermore, the activation of leached Ti-Mnt did not improve significantly the Pb²⁺ adsorption capability, implying that the activation process is not necessary for the recycling of Ti-Mnt.

Table 2. Adsorption data and interlayer distances for Na-Mnt and Ti-Mnt.

Sample name	C_0 (mg/L)	C_1 (mg/L)	Adsorption capability (%)	Uncertainty (%)	d_{001} (nm)
Na-Mnt	1000	11.4	88.6	±0.1	1.219
Ti-Mnt	1000	nd	99.9	±0.1	1.529

nd: below the detection limit (0.1 mg/L); C_0 : initial concentration of Pb²⁺; C_1 : equilibrium concentration of Pb²⁺ in the aqueous solution.

Table 3. Leaching data for Ti-Mnt.

Sample name	$C_0 - C_1$ (mg/L)	C_2 (mg/L)	Leaching ratio (%)	Uncertainty (%)
Ti-Mnt	1000	848	84.8	±0.1

C_0 : initial concentration of Pb²⁺; C_1 : the equilibrium concentration of Pb²⁺; C_2 : the concentration of Pb²⁺ in the nitric acid solution after leaching.

Table 4. Comparative data for adsorption experiments.

Sample name	C_0 (mg/L)	C_2 (mg/L)	Adsorption capability (%)	Uncertainty (%)
Ti-Mnt	100	nd	99.9	±0.1
Sample 1	100	4.3	95.7	±0.1
Sample 2	100	4.0	96.0	±0.1

nd is below the detection limit (0.1 mg/L); C_0 : initial concentration; C_2 : concentration of Pb^{2+} in the nitric acid solution after adsorption.

Relationship between microstructure and adsorption capability

The relationship between the Pb^{2+} adsorption capability and the interlayer spacing of Mnt indicated that the adsorption capability could be improved by pillaring with anatase (Figure 6). The Pb^{2+} adsorption capability of Ti-Mnt first increased with its interlayer spacing and then decreased when the spacing reached 1.529 nm. This suggests that the interlayer spacing is not the only factor that determines the Pb^{2+} adsorption capability of Ti-Mnt. In particular, when the Pb^{2+} adsorption capability of Ti-Mnt was >99.9%, the corresponding basal (001) spacings were 1.414 nm and 1.437 nm (Figure 6). The basal spacing was neither the largest nor the smallest among the five samples (Figure 6). In addition, the specific surface areas of these two samples, the basal (001) spacings of which were 1.414 nm and 1.437 nm, were at medium levels compared with all the others of the five samples (Table 1), and their layer structures were loose (Figures 4, 5). Anatase particles in these two samples were well distributed and located in both the interlayer space of the (001) plane and beyond the interlayer space of Ti-Mnt (Figure 5e, f). In these cases, sufficient interlayer space and well-dispersed anatase particles provided enough space to adsorb Pb^{2+} from the aqueous solution. Furthermore, the basal surface of Mnt containing efficient active sites for adsorbing metal ions can be

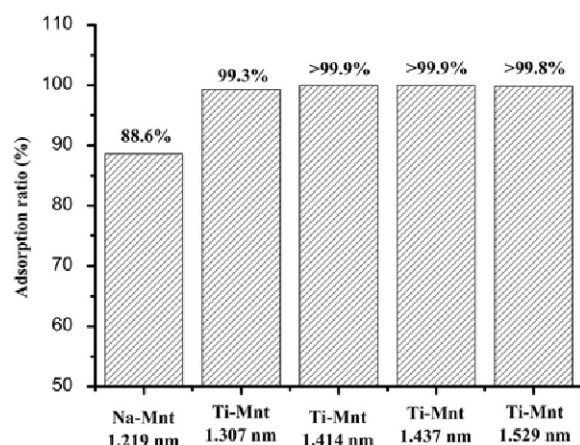


Figure 6. Relationship between adsorption ability and interlayer spacing of the samples.

exposed sufficiently (Underwood *et al.*, 2016). Therefore, the Ti-Mnt exhibited very well the adsorption capability.

Overall, the results indicated that the Pb^{2+} adsorption capability of Ti-Mnt is related to the interlayer spacing of Mnt, the distribution of anatase particles pillared in Mnt, and the specific surface area. Neither a linear relationship between Pb^{2+} adsorption ability and specific surface area of Ti-Mnt, nor a linear relationship between Pb^{2+} adsorption ability and the interlayer spacing of the (001) plane of Ti-Mnt was found.

CONCLUSIONS

Anatase was pillared successfully in the interlayer space of Na-Mnt. The Pb^{2+} adsorption capability of Ti-Mnt is related to the interlayer spacing of Mnt, the distribution of anatase particles, and the specific surface area. The improvement in Pb^{2+} adsorption capability is related to the enlarged interlayer spacing and to the loose layer structure of the (001) plane of Mnt, as well as well dispersed anatase particles and sufficient adsorptive active sites provided by both the Mnt layers and anatase particles. In addition, the Pb^{2+} adsorbed in Ti-Mnt could be leached by nitric acid solution, demonstrating that the Ti-Mnt can be recycled easily and utilized to recover lead metal resources from industrial sewage. These findings could be exploited to adjust the Pb^{2+} adsorption capability of other inorganic nanocomposites with lamellar structures and set a basic foundation for the application of Mnt in environmental protection.

ACKNOWLEDGMENTS

This research was supported by the National Natural Science Foundation of China (21173193 and 21301154); Natural Science Foundation of Zhejiang Province (406094 and Q19B010009), P.R. China; the Scientific and Technical Project of Zhejiang Province (2009R50002-15 and 2013C37104), P.R. China; and the Scientific and Technical Projects of Education Department of Zhejiang Province (Y201225711), P.R. China.

REFERENCES

- Barama, S., Davidson, A., Barama, A., Boukhlof, H., Casale, S., Calers, C., Brouri, D., Domingos, C., and Djadoun, A. (2017) Dephosphatation under UV light of water by Ti-PILC with activation by secondary species (La, Se, and Rb).

- Comptes Rendus Chimie*, **20**, 7–19.
- Chen, D.M., Du, G.X., Zhu, Q., and Zhou, F.S. (2013) Synthesis and characterization of TiO₂ pillared montmorillonites: application for methylene blue degradation. *Journal of Colloid and Interface Science*, **409**, 151–157.
- Djellabi, R., Ghorab, M.F., Cerrato, G., Morandi, S., Gatto, S., Oldani, V., Michele, A.D., and Bianchi, C.L. (2014) Photoactive TiO₂-Mnt composite for degradation of organic dyes in water. *Journal of Photochemistry and Photobiology A: Chemistry*, **295**, 57–63.
- Fetter, G., Heredia, G., Velázquez, L.A., Maubert, A.M., and Bosch, P. (1997) Synthesis of aluminum-pillared montmorillonites using highly concentrated clay suspensions. *Applied Catalysis A: General*, **162**, 41–45.
- Hur, S.G., Kim, T.W., Hwang, S.J., Hwang, S.H., Yang, J.H., and Choy, J.H. (2006) Heterostructured nanohybrid of zinc oxide-Mnt clay. *Journal of Physical Chemistry B*, **110**, 1599–1604.
- Irannajad, M. and Haghghi, H.K. (2017) Removal of Co²⁺, Ni²⁺, and Pb²⁺ by manganese oxide-coated zeolite: equilibrium, thermodynamics, and kinetics studies. *Clays and Clay Minerals*, **65**, 52–62.
- Korosi, L., Nemeth, J., and Dekany, I. (2004) Structural and photooxidation properties of SnO₂/layer silicate nanocomposites. *Applied Clay Science*, **27**, 29–40.
- Liang, K. (2013) A study on absorption of titania pillared Mnt for heavy metal ions. *Acta Mineralogica Sinica*, **33**, 408–414.
- Miao, S.D., Liu, Z.M., Han, B.X., Yang, H.W., Miao, Z.J., and Sun, Z.Y. (2006) Synthesis and characterization of ZnS-Mnt nanocomposites and their application for degrading eosin B. *Journal of Colloid and Interface Science*, **301**, 116–122.
- Mogyorosi, K., Dekany, I., and Fendler, J.H. (2003) Preparation and characterization of clay mineral intercalated titanium dioxide nanoparticles. *Langmuir*, **19**, 2938–2946.
- Mulewa, W., Tahir, M., and Amin, N.A.S. (2017) MNT-supported Ni/TiO₂ nanocomposite for low temperature ethanol steam reforming toward hydrogen production. *Chemical Engineering Journal*, **326**, 956–969.
- Ooka, C., Yoshida, H., Horio, M., and Hattori, T. (2003) Adsorptive and photocatalytic performance of TiO₂ pillared Mnt in degradation of endocrine disruptors having different hydrophobicity. *Applied Catalysis B: Environmental*, **41**, 313–321.
- Sun, H.J., Peng, T.J., Liu, B., and Xian, H.Y. (2015) Effects of montmorillonite on phase transition and size of TiO₂ nanoparticles in TiO₂/Mnt nanocomposites. *Applied Clay Science*, **114**, 440–446.
- Tabet, D., Saidi, M., Houari, M., Pichat, P., and Khalaf, H. (2006) Fe-pillared clay as a Fenton-type heterogeneous catalyst for cinnamic acid degradation. *Journal of Environmental Management*, **80**, 342–346.
- Tahir, M. and Amin, N.A.S. (2013) Photocatalytic reduction of carbon dioxide with water vapors over montmorillonite-modified TiO₂ nanocomposites. *Applied Catalysis B: Environmental*, **142–143**, 512–522.
- Tahir, M., Tahir, B., and Amin, N.S. (2015) Photocatalytic CO₂ reduction by CH₄ over montmorillonite-modified TiO₂ nanocomposites in a continuous monolith photoreactor. *Materials Research Bulletin*, **63**, 13–23.
- Underwood, T., Erastova, V., and Greenwell, H.C. (2016) Ion adsorption at clay-mineral surfaces: the Hofmeister series for hydrated smectite minerals. *Clays and Clay Minerals*, **64**, 472–487.
- Yaron-Marcovich, D., Chen, Y., Nir, S., and Prost, R. (2005) High resolution electron microscopy structural studies of organo-clay nanocomposites. *Environmental Science & Technology*, **39**, 1231–1238.
- Zhang, P., Mo, Z.L., Han, L.J., Zhu, X.B., Wang, B., and Zhang, C. (2014) Preparation and photocatalytic performance of magnetic TiO₂/Mnt/Fe₃O₄ nanocomposites. *India Engineering Chemical Research*, **53**, 8057–8061.
- Zhou, C.H. (2011) An overview on strategies towards clay-based designer catalysts for green and sustainable catalysis. *Applied Clay Science*, **53**, 87–96.
- Zhou, C.H. and Keeling, J. (2013) Fundamental and applied research on clay minerals: From climate and environment to nanotechnology. *Applied Clay Science*, **74**, 3–9.
- Zhou, C.H., Zhao, L.Z., Wang, A.Q., Chen, T.H., and He, H.P. (2016) Current fundamental and applied research into clay minerals in China. *Applied Clay Science*, **119**, 3–7.

(Received 14 November 2017; revised 31 August 2018; Ms. 1237; AE: Chun-Hui Zhou)